

Magnetic structure and orbital ordering in KCrF_3 perovskite

Y. Xiao,^{1,*} Y. Su,² H.-F. Li,^{1,3} C.M.N. Kumar,¹ R. Mittal,^{2,4} J. Persson,¹ A. Senyshyn,^{5,6} K. Gross,¹ and Th. Brueckel^{1,2}

¹*Institut fuer Festkoerperforschung, Forschungszentrum Juelich, D-52425 Juelich, Germany*

²*Juelich Centre for Neutron Science, IFF, Forschungszentrum Juelich, Outstation at FRM II, Lichtenbergstr. 1, D-85747 Garching, Germany*

³*Ames Laboratory and Department of Physics and Astronomy, Iowa State University, Ames, Iowa 50011, USA*

⁴*Solid State Physics Division, Bhabha Atomic Research Centre, Trombay, Mumbai 400085, India*

⁵*Institute for Materials Science, Darmstadt University of Technology, D-64287 Darmstadt, Germany*

⁶*Forschungsneutronenquelle Heinz Maier-Leibnitz (FRM II), D-85747 Garching, Germany*

(Dated: August 18, 2018)

KCrF_3 represents another prototypical orbital-ordered perovskite, where Cr^{2+} possesses the same electronic configuration of $3d^4$ as that of strongly Jahn-Teller distorted Mn^{3+} in many CMR manganites. The crystal and magnetic structures of KCrF_3 compound are investigated by using polarized and unpolarized neutron powder diffraction methods. The results show that the KCrF_3 compound crystallizes in tetragonal structure at room temperature and undergoes a monoclinic distortion with the decrease in temperature. The distortion of the crystal structure indicates the presence of cooperative Jahn-Teller distortion which is driven by orbital ordering. With decreasing temperature, four magnetic phase transitions are observed at 79.5, 45.8, 9.5, and 3.2 K, which suggests a rich magnetic phase diagram. Below $T_N = 79.5$ K, the Cr^{2+} moment orders in an incommensurate antiferromagnetic arrangement, which can be defined by the magnetic propagation vector $(\frac{1}{2} \pm \delta, \frac{1}{2} \pm \delta, 0)$. The incommensurate-commensurate magnetic transition occurs at 45.8 K and the magnetic propagation vector locks into $(\frac{1}{2}, \frac{1}{2}, 0)$ with the Cr moment of $3.34(5) \mu_B$ aligned ferromagnetically in (220) plane, but antiferromagnetically along [110] direction. Below 9.5 K, the canted antiferromagnetic ordering and weak ferromagnetism arise from the collinear antiferromagnetic structure, while the Dzyaloshinskii-Moriya interaction and tilted character of the single-ion anisotropy might give rise to the complex magnetic behaviors below 9.5 K.

PACS numbers: 75.25.Dk, 75.25.-j, 75.50.Ee, 71.70.Ej

The strongly correlated electron systems such as $3d$ transition metal oxides have attracted considerable attention due to their complex structural, electronic and magnetic characteristics [1, 2]. The interactions between lattice, spin and orbital degrees of freedom are considered to play the essential role in explaining some interesting physical properties [3]. For example, the colossal magnetoresistance (CMR) effect was observed in hole-doped perovskite manganites such as $\text{La}_{1-x}\text{M}_x\text{MnO}_3$ ($M = \text{Sr}, \text{Ca}$ and Ba) [4–7]. While the undoped parent compound LaMnO_3 is known to be an A-type antiferromagnetic (AFM) insulator in which the orbital ordering is formed due to the cooperative Jahn-Teller (JT) effect. The electronic configuration of Mn^{3+} ions in LaMnO_3 is $t_{2g}^3 e_g^1$ by using the Hund's rule as a first approximation. The three electrons in the t_{2g} orbitals are localized with a total spin $3/2$ while the electron in the e_g atomic orbitals is strongly hybridized with the neighboring oxygen p orbitals. This particular orbital ordering is responsible for the A-type antiferromagnetic structure of LaMnO_3 [8]. The mixed valence ($\text{Mn}^{3+}\text{Mn}^{4+}$) will be formed with the hole doping on the e_g band. It is believed that the CMR effect is due to the double exchange of electrons between ferromagnetically coupled Mn^{3+} and Mn^{4+} ions [4]. Therefore, the interplay and coupling between the lattice, orbital and spin degrees of freedom are interesting and deserve to be investigated from both the fundamental and technical point of view.

Besides the transition metal oxides, the transition metal fluorides also exhibit the intriguing electronic and magnetic effects. However, compared with the extensive study of oxides,

the study of fluorides is still lack due to the difficulty of synthesis. KCrF_3 is one kind of perovskite structure fluorides in which the electronic and structural characteristics is expected to resemble with those of widely studied LaMnO_3 compounds since the orbital degrees of freedom are activated for Cr^{2+} (d^4) cation. Recently, the crystal structure and magnetic properties of KCrF_3 compound were investigated by synchrotron x-ray powder diffraction and magnetic measurements [9]. Both the structural and magnetic phase transitions seem to be more complex than expected. The KCrF_3 displays not only the large cooperative Jahn-Teller distortions at room temperature but also a series of temperature induced structural and magnetic transformations. However, the detailed magnetic structure of KCrF_3 is still not studied systematically. To clarify the magnetic ordering is of important significance to understand the interactions between the lattice, spin and orbital degrees of freedom in KCrF_3 .

In this paper, we have studied both the cooperative Jahn-Teller distortion and magnetic phase transition of KCrF_3 by using polarized and unpolarized neutron powder diffraction (NPD) methods. We have observed series of magnetic phase transitions including an incommensurate-commensurate magnetic phase transition. The magnetic phase diagram of KCrF_3 is presented based on the magnetization, heat capacity and NPD measurements between 2.5 and 300 K.

Polycrystalline KCrF_3 sample was prepared by standard solid state reaction method. The stoichiometric powders of KF and CrF_2 were mixed, pressed into pellets and sealed in an evacuated quartz tube, followed by sintering at 700 K for

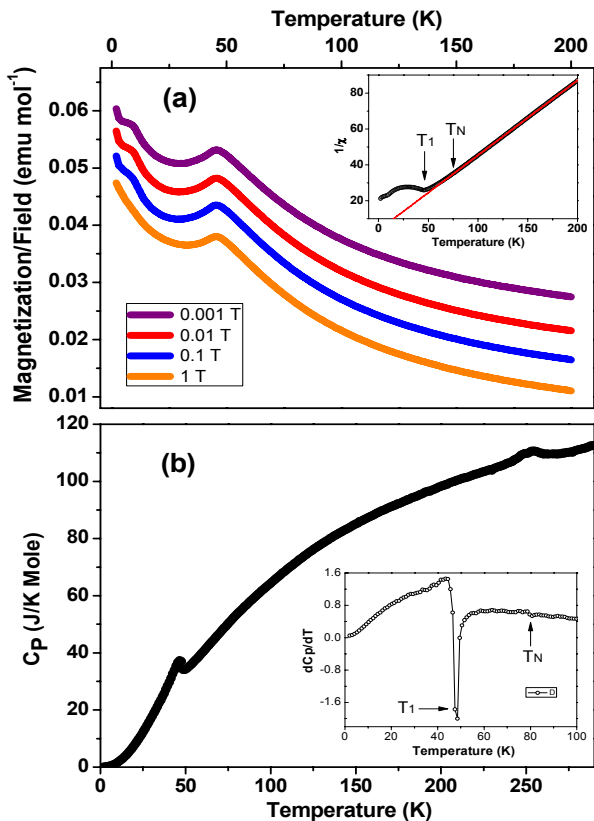


FIG. 1: (Color online) (a) Temperature dependence of the magnetization of KCrF_3 measured in zero-field-cooling mode under different magnetic fields. In order to clearly show the change of magnetic features, the unit is allocated only to magnetization curve measured with applied field of 1 T, while the rest three curves (with fields equal to 0.001, 0.01 and 0.1 T) are shifted upwards. The inset shows the temperature vs. inverse susceptibility of KCrF_3 measured at magnetic field of 0.1 T. (b) Temperature dependence of heat capacity of KCrF_3 . Inset: dC_p/dT emphasizes breaks in slope of $C_p(T)$ data.

24 h with one intermediate grinding. All the weighting, mixing and pressing procedures were performed in a MBRAUN-MB20G glove box with a protective argon atmosphere. The laboratory x-ray diffraction measurement reveals that single phase was obtained with small amount of Cr_2O_3 impurities ($\sim 2\%$). Temperature dependence of both magnetization and specific heat were collected by using a Quantum Design Magnetic Properties Measurement System (MPMS) and a Physical Properties Measurement System (MPMS), respectively, with temperature down to 2 K. Neutron diffraction measurements were performed on the high resolution diffractometer SPODI and the diffuse neutron scattering spectrometer DNS at FRMII (Munich, Germany). For the NPD measurement on SPODI, a Ge(551) monochromator was used to produce a monochromatic neutron beam of wavelength 1.5481 Å. The polarized analysis was performed on DNS with the polarized neutron beam of wavelength 4.74 Å. The program FULLPROF [10] was used for the Rietveld refinement of the crystal and the magnetic structures of the compounds.

The temperature dependence of the magnetization of the KCrF_3 sample was measured under different magnetic fields as shown in Fig. 1(a). Three phase transitions are clearly visible at 45.8 K (T_1), 9.5 K (T_2) and 3.2 K (T_3). The similar discontinuities in the M - T curve are also reported in previous literatures [9, 11] and the anomaly at 45.8 K was considered as the Neel temperature T_N where the paramagnetic state develops from the antiferromagnetic phase with increasing temperature. However, in present work the polarized neutron analysis experiment indicated that the kink at 45.8 K corresponds to a commensurate-incommensurate antiferromagnetic phase transition and the system enters the paramagnetic state at a higher temperature of 79.5 K, as discussed in the following text. It is also noticed that the anomalies at 9.5 and 3.2 K are not shown by applying higher magnetic field of 1 T which is the signature of the field-induced magnetic phase transition. The inset of Fig. 1(a) shows the temperature dependence of the inverse susceptibility $1/\chi$ of the compound measured under magnetic field of 0.1 T. The susceptibility strictly follows the Curie-Weiss behavior above 80 K. The effective paramagnetic moment and Weiss temperature are deduced to be $4.379(1) \mu_B$ and $-8.7(4)$ K, respectively. It is noticed that a positive Weiss temperature (~ 2.7 K) is given in Ref.[9] based on the analysis of magnetic susceptibility χ which is measured in an applied field of 1 T. It is known that Curie-Weiss law is only valid with low applied field and too strong field may affect considerably the susceptibility by changing the weak electron coupling and leading to magnetic saturation. Therefore, the different Weiss temperatures obtained for KCrF_3 are attributed to different measuring conditions and the Weiss temperature deduced with lower field measurement reflects the antiferromagnetic background magnetism in KCrF_3 . Fig. 1(b) shows the temperature dependence of the heat capacity result in which a clear phase transition is detected at 248 K. The crystal structure analysis given below reveals that the kink at 248 K is associated with the monoclinic to tetragonal crystal structural phase transition. Another phase transition at 79.5 K can be more clearly identified by examining the dC_p/dT plot as shown in the inset of Fig. 1(b). Therefore, a series of phase transitions in KCrF_3 are constructed by magnetic and thermal characterizations, which suggest a rich phase diagram of KCrF_3 .

The neutron powder diffraction pattern of KCrF_3 at 300 K is shown in Fig. 2(a). The compound crystallizes in the tetragonal phase with space group $I4/mcm$. The lattice parameters are deduced to be $a = 6.0464(6)$ Å and $c = 8.0230(8)$ Å, which is in good agreement with that derived from synchrotron x-ray powder diffraction [9]. The detailed structural information for KCrF_3 , as obtained from NPD data, are given in Table I. The crystal structure can be described as the stacking of layers of corner-sharing CrF_6 octahedra. In the ab plane the CrF_6 octahedra are elongated along the a or b axis in an alternative pattern. The structure distortion is caused by the orbital order associated with the cooperative Jahn-Teller distortion, *i.e.* the $d_{3x^2-r^2}/d_{3y^2-r^2}$ orbitals are stabilized by the Jahn-Teller distor-

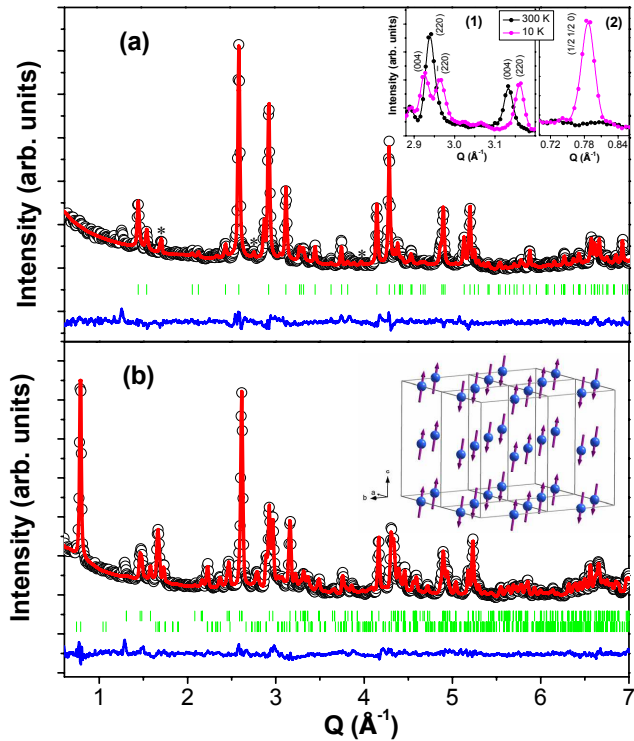


FIG. 2: (Color online) (a) NPD refinement pattern for the KCrF_3 at 300 K. The vertical bars at the bottom indicate the Bragg reflection positions, and the lowest curve is the difference between the observed and the calculated NPD patterns. Cr_2O_3 impurities are marked with asterisks. The Inset (1) and (2) show the splitting of tetragonal (220) peak and the onset of $(\frac{1}{2}\frac{1}{2}0)$ magnetic reflection at low temperature, respectively. (b) NPD refinement pattern for the KCrF_3 at 10 K. Inset shows the magnetic structure of KCrF_3 at 10 K. Frames indicate the crystallographic unit cells and the magnetic unit cell doubled along both a and b directions.

tion and order in an alternate staggered pattern in the ab plane as illustrated in Fig. 3(a). Similar to the MnO_6 octahedral distortion in LaMnO_3 [12, 13], there also exist three Cr-F distances in KCrF_3 named short L_s , medium L_m and long L_l . The magnitude of the Jahn-Teller distortion of CrF_6 can be evaluated by the following equation: $\Delta = (1/6)\sum[(d_n - \langle d \rangle)/\langle d \rangle]^2$, where $\langle d \rangle$ and d_n are the mean Cr-F bond length and the six Cr-O bond lengths along six different directions, respectively. The calculated value of Δ is 4.87×10^{-3} for KCrF_3 at 300 K. With decreasing temperature, the KCrF_3 undergoes a monoclinic phase transition as revealed by the NPD pattern at 10 K. The inset(1) of Fig. 2(a) shows the obvious splitting of the tetragonal (220) peak into the monoclinic (220) and $(\bar{2}20)$ peaks. Along with the monoclinic distortion, two inequivalent Cr sites ($2c$ and $2d$) form with similar octahedral environment. The Jahn-Teller distortion parameter was deduced to be 5.66×10^{-3} and 3.85×10^{-3} for $2d$ and $2c$ CrF_6 octahedra, respectively. The alternated arrangement of CrF_6 octahedra within the ab plane also indicates the change in orbital ordering as illustrated in Fig. 3(b). However, it should be noted that the change in magnetic order and the change in orbital or-

TABLE I: Refined results of the crystal and magnetic structures for KCrF_3 at 10 and 300 K. The atomic positions for space group $I112/m$: $\text{K}(4g)(0,0,z)$, $\text{Cr}_{(1)}(2c)(0,0.5,0)$, $\text{Cr}_{(2)}(2d)(0,0.5,0.5)$, $\text{F}_{(1)}(4i)(x,y,0)$, $\text{F}_{(2)}(4i)(x,y,0)$, $\text{F}_{(3)}(4h)(0,0.5,z)$; for $I4/mcm$: $\text{K}(4a)(0,0,0.25)$, $\text{Cr}_{(1)}(4d)(0,0.5,0)$, $\text{F}_{(1)}(4b)(0,0.5,0.25)$, $\text{F}_{(2)}(8h)(x,y,0)$.

Temperature	10 K	300 K
Space group	$I112/m$	$I4/mcm$
a (\AA)	5.8069(7)	6.0464(6)
b (\AA)	5.8137(7)	6.0464(6)
c (\AA)	8.5871(7)	8.0230(8)
γ ($^\circ$)	93.671(5)	90
V (\AA^3)	289.303(2)	293.312(2)
K		
z	0.247(2)	0.25
B (\AA^2)	1.3(2)	2.4(2)
$\text{Cr}_{(1)}$		
B (\AA^2)	1.1(2)	1.8(1)
$M(\mu_B)$	3.34(5)	
$\text{Cr}_{(2)}$		
B (\AA^2)	1.4(2)	
$M(\mu_B)$	3.34(5)	
$\text{F}_{(1)}$		
x	0.291(2)	0
y	0.718(2)	0.5
B (\AA^2)	1.6(2)	3.0(2)
$\text{F}_{(2)}$		
x	0.230(2)	0.231(2)
y	0.197(2)	0.731(2)
B (\AA^2)	1.7(2)	2.6(2)
$\text{F}_{(3)}$		
z	0.230(2)	
B (\AA^2)	1.7(2)	
R_p	2.76	2.70
R_{wp}	3.56	3.51
χ^2	3.51	3.35

der took place at different temperatures, *i.e.* there is no direct correlation between orbital ordering and magnetic ordering in KCrF_3 . The correlation between magnetic ordering and orbital ordering are also investigated in LaMnO_3 by Subías *et al.* [14] with resonant x-ray scattering method, which can act as a direct probe for orbital ordering. Their experimental results also indicated that there is no correlation between resonant scattering and long-range AFM ordering in LaMnO_3 .

Besides the crystal structural phase transition, the magnetic phase transition is also observed at 10 K due to the ordering of the Cr^{2+} moments as revealed by the onset of magnetic reflection (inset(2) in Fig. 2(a)). The magnetic reflection at $Q = 0.7904 \text{ \AA}^{-1}$ can be indexed accurately with $(\frac{1}{2}\frac{1}{2}0)$ instead of (001) magnetic reflection [15] although the d values of those two reflections are quite close. It strongly indicated that the moments of Cr^{2+} formed antiferromagnetic structure with $(\frac{1}{2}, \frac{1}{2}, 0)$ magnetic modulation. Also, the existence of considerable intensity of $(\frac{1}{2}\frac{1}{2}2)$ magnetic reflection indicates that the Cr^{2+} moment tilts outward c axis. By performing refine-

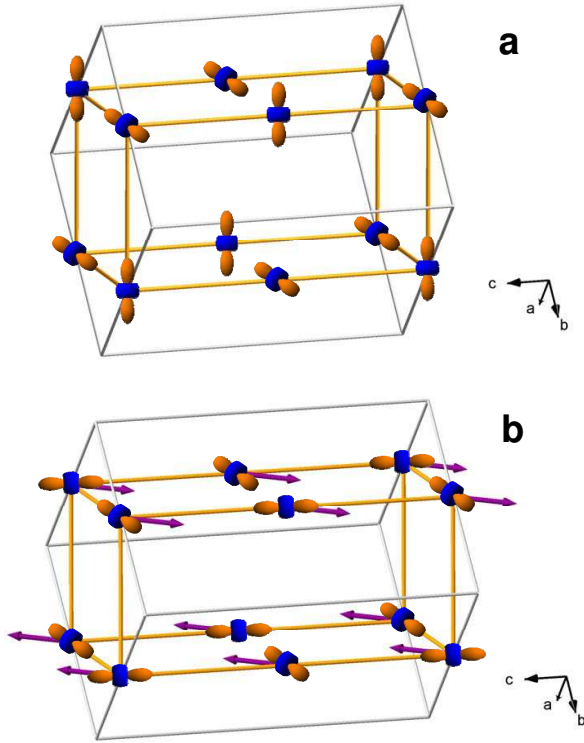


FIG. 3: (Color online) Schematic view of the orbital and spin ordering in the perovskite chromite KCrF_3 of tetragonal (a) and monoclinic (b) phases. The grey line outlines the unit cell.

ment on the NPD data, we found that the magnetic structure of KCrF_3 can be described by the collinear antiferromagnetic structure model, *i.e.* the KCrF_3 system develops a long-range antiferromagnetic order at 10 K with the Cr^{2+} spins coupled ferromagnetically in the (220) plane and antiferromagnetically along the [110] direction as shown in the inset of Fig. 2(b). The moment of Cr^{2+} at 10 K is deduced to be $3.34(5) \mu_B$ which is close to the theoretical value [16, 17]. Similar to the A-type AFM in LaMnO_3 [8, 18, 19], the layered AFM structure of KCrF_3 can also be considered as the consequence of an interplay between superexchange and Jahn-Teller coupling. According to the Goodenough-Kanamori-Anderson (GKA) rules [20–24], the superexchange between magnetic ions is mediated by the F ligand and the FM coupling is expected due to the superexchange interaction between the filled e_g and empty orbitals, while the AFM coupling is expected due to the superexchange interaction between the unfilled orbitals. Our experimental results confirmed the picture of the interactions between magnetic ordering and orbital ordering given by the GKA rules. The schematic view of the orbital ordering and spin ordering in the unit cell of monoclinic KCrF_3 is shown in Fig. 3(b).

In order to inspect the evolution of the magnetic ordering and clarify magnetic structure of the KCrF_3 system, neutron polarization analysis was performed at DNS in the Q range from 0.346 to 2.29 \AA^{-1} and temperature range from 2.5 to

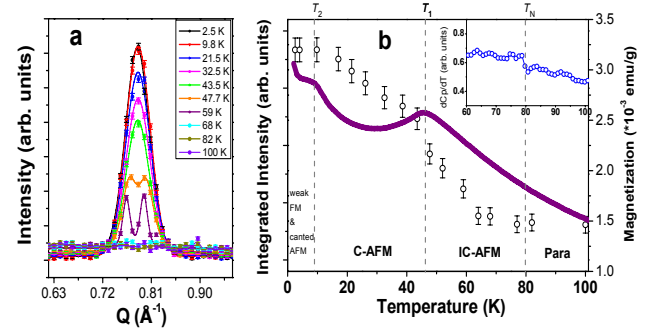


FIG. 4: (Color online) (a) Evolution of the $(\frac{1}{2}\frac{1}{2}0)$ magnetic reflection with the change of temperature. (b) Magnetic phase diagram of KCrF_3 . The open circle and purple curve represent the temperature dependences of integrated intensity of $(\frac{1}{2}\frac{1}{2}0)$ magnetic reflection and magnetization, respectively. The inset shows the enlarged view of the slope of C_p data.

100 K with smaller temperature steps. The nuclear coherent, spin-incoherent and magnetic scattering cross sections can be separated with the xyz -polarization method in the spin-flip and non-spin-flip channels with polarized analysis[25]. At 9.8 K, magnetic reflections are clearly seen and match with the presented AFM structure model. The evolution of the $(\frac{1}{2}\frac{1}{2}0)$ magnetic reflection is plotted in Fig. 4(a) and the integrated intensity of $(\frac{1}{2}\frac{1}{2}0)$ magnetic reflection in Fig. 4(b) as the open circles. Here we will discuss the magnetic structure below 10 K firstly. Compared to the $(\frac{1}{2}\frac{1}{2}0)$ reflection at 9.8 K, no obvious change in integrated intensity was detected for the $(\frac{1}{2}\frac{1}{2}0)$ reflection at 4.0 and 2.5 K, which may suggest a slight canting of the magnetic moment of Cr^{2+} ions outward the (220) ferromagnetic plane. It is known that canted AFM and weak FM moment are observed in both noncrystalline and single crystal LaMnO_3 samples [26, 27]. The FM moment in LaMnO_3 is caused by the tilt of Mn^{3+} moments away from the AFM ab plane resulting in a net magnetization along c axis [27, 28]. Considering the structural comparability between the KCrF_3 and LaMnO_3 systems, the increasing magnetization below 9.5 K in KCrF_3 may arise due to the tilt of the Cr^{2+} moment out of the (220) plane. Both the Dzyaloshinskii-Moriya (DM) exchange interaction and the character of the single-ion anisotropy are necessary to give an explanation on that weak ferromagnetism [27–30]. Therefore, the magnetic structure below 9.5 K is associated with the mixed state of weak FM and canted AFM configurations. The neutron diffraction analysis on KCrF_3 single crystal is required to explore the exact magnetic structure of KCrF_3 below 10 K and to illustrate the nature of phase transition at 3.2 K.

Now we discuss the magnetic structure above 10 K. As shown in Fig. 4(a), the intensity of the $(\frac{1}{2}\frac{1}{2}0)$ magnetic reflection decreases gradually with increasing temperature from 9.8 K, which suggests the decrease of amplitude of the Cr^{2+} moment. At 47.7 K, two satellite reflections are developed instead of the single $(\frac{1}{2}\frac{1}{2}0)$ reflection. It suggests that the transition at 45.8 K corresponds to the magnetic phase transition

from simple collinear AFM phase to an incommensurate magnetic phase with the propagation vector $(\frac{1}{2} \pm \delta, \frac{1}{2} \pm \delta, 0)$. As an example, the magnetic propagation wave vector q is deduced to be $(\frac{1}{2} \pm 0.01, \frac{1}{2} \pm 0.01, 0)$ for KCrF_3 at 47.7 K. However, regarding to the propagation vector $(\frac{1}{2} \pm \delta, \frac{1}{2} \pm \delta, 0)$, there exist several possible magnetic structural schemes including the sinusoidal and helimagnetic solutions. Polarized neutron experiments on the KCrF_3 single crystals may shed light on the nature of that incommensurate magnetic structure. Usually, the presence of modulated phases is the consequence of the competing next nearest-neighbor exchange interaction and anisotropy in the spin Hamiltonian [31, 32]. In the monoclinic phase of KCrF_3 , the tilt of CrF_6 octahedra lead to a nonzero angle between the occupied e_g orbital and the (220) plane. As a result, the Cr-F-Cr superexchange angle deviates from 180° and probably weakens the FM interactions between Cr^{2+} and four nearest neighbor Cr^{2+} ions inside the (220) plane. The next nearest-neighbor exchange may play a role to stabilize the incommensurate AFM state. The paramagnetic state is established when the sample is heated up to 82 K. The Neel temperature T_N (79.5 K) is clearly defined by the distinct anomaly in the slope of the C_P data as shown in the inset of Fig. 4b.

In summary, we have investigated the correlation among the structural transition, orbital ordering and magnetic ordering in perovskite chromite KCrF_3 . In this system, two different orbital ordering states are observed below and above the structural transition temperature. With decreasing temperature, the incommensurate A-type AFM state emerges firstly due to the ordering of the moment of Cr^{2+} and the commensurate AFM order develops from the incommensurate AFM state at 45.8 K with a magnetic propagation vector change from $(\frac{1}{2} \pm \delta, \frac{1}{2} \pm \delta, 0)$ to $(\frac{1}{2}, \frac{1}{2}, 0)$. The noncollinear canted magnetic structure and weak ferromagnetic structure might be the nature of lower temperature phase zone. The rich magnetic phase diagram with various commensurate and incommensurate phases is ascribed to competing nearest-neighbor and next nearest-neighbor exchange interactions, single ion anisotropy as well as the DM interaction.

The authors are grateful to P. Meuffels and H. Bierfeld for providing assistance with sample preparation. We also thank E. Kentzinger and B. Schmitz for the help with the magnetization and heat capacity measurements.

* Electronic address: y.xiao@fz-juelich.de

- [1] M. Imada, A. Fujimori, and Y. Tokura, The Physics of manganites: Structure and transport. Rev. Mod. Phys. **70**, 1039 (1998).
 [2] P. A. Lee, N. Nagaosa, and X. Wen, Doping a Mott insula-

- tor: Physics of high-temperature superconductivity. Rev. Mod. Phys. **78**, 17 (2006).
 [3] Y. Tokura and N. Nagaosa, Orbital Physics in Transition-Metal Oxides. Science, **288**, 462 (2000).
 [4] Y. Tokura, Rep. Prog. Phys. **69**, 797 (2006).
 [5] A. Asamitsu, Y. Moritomo, Y. Tomioka, T. Arima, and Y. Tokura, Nature(London) **373**, 407 (1995).
 [6] S. Jin, M. McCormack, T.H. Tiefel, and R. Ramesh, J. Appl. Phys. **76**, 6929 (1994).
 [7] R. von Helmolt, J. Wecker, B. Holzapfel, L. Schultz, and K. Samwer, Phys. Rev. Lett. **71**, 2331 (1993).
 [8] E. O. Wollan and W. C. Koehler, Phys. Rev. **100**, 545 (1955).
 [9] S. Margadonna and G. Karotsis, J. Am. Chem. Soc. **128**, 16436 (2006).
 [10] J. Rodríguez-Carvajal, Physica B **192**, 55 (1993).
 [11] S. Yoneyama, K. Hirakawa, J. Phys. Soc. Jpn. **21**, 183 (1966).
 [12] T. Chatterji, P. F. Henry, and B. Ouladdiaf, Phys. Rev. B **77**, 212403 (2008).
 [13] J. Rodríguez-Carvajal, M. Hennion, F. Moussa, A. H. Moudén, L. Pinsard, and A. Revcolevschi, Phys. Rev. B **57**, R3189 (2008).
 [14] G. Subías, J. Herrero-Martín, J. García, J. Blasco, C. Mazzoli, K. Hatada, S. Di Matteo, and C. R. Natoli, Phys. Rev. B **75**, 235101 (2007).
 [15] V. Scaturin, L. Corliss, N. Elliott, J. Hastings, Acta Crystallogr. **14**, 19 (1961).
 [16] Gianluca Giovannetti, Serena Margadonna, and Jeroen van den Brink, Phys. Rev. B **77**, 075113 (2008).
 [17] Yuanhui Xu, Xianfeng Hao, Minfeng Lv, Zhijian Wu, Defeng Zhou, and Jian Meng, J. Chem. Phys. **128**, 164721 (2008).
 [18] Igor Solovyev, Noriaki Hamada, and Kiyoyuki Terakura, Phys. Rev. Lett. **76**, 4825 (1996).
 [19] D. Feinberg, P. Germain, M. Grilli, and G. Seibold, Phys. Rev. B **57**, R5583 (1998).
 [20] J. Kanamori, J. Phys. Chem. Solids **10**, 87 (1959).
 [21] P. W. Anderson, Phys. Rev. **109**, 1492 (1958).
 [22] J. B. Goodenough, *Magnetism and the Chemical Bond* (Interscience Publ., New York, 1963).
 [23] K. I. Kugel and D. I. Khomskii, Zh. Eksp. Teor. Fiz. **64**, 1429 (1973) [Sov. Phys. JETP **37**, 725 (1973)]
 [24] D. I. Khomskii and K. I. Kugel, Phys. Rev. B **67**, 134401 (2003).
 [25] W. Schweika and P. Böni, Physica B **297**, 155 (2001).
 [26] G. Matsumoto, J. Phys. Soc. Jpn. **29**, 606 (1970).
 [27] V. Skumryev, F. Ott, J. M. D. Coey, A. Anane, J. P. Renard, L. Pinsard-Gaudart, and A. Revcolevschi, Eur. Phys. J. B. **11**, 401 (1999).
 [28] Diyar Talbayev, László Mihály, and Jianshi Zhou, Phys. Rev. Lett. **93**, 017202 (2004).
 [29] T. Moriya, in *Magnetism*, Edited by G. T. Rado and H. Suhl, (Academic Press, New York, 1984).
 [30] I. Dzyaloshinski, J. Phys. Chem. Solids **4**, 241 (1958).
 [31] J. Kocinski, *Commensurate and Incommensurate Phase Transitions* (Elsevier, Amsterdam, 1990).
 [32] P. Bak, Rep. Prog. Phys. **45**, 587 (1982).